RESEARCH ARTICLE | JANUARY 13 2026

The application of a fluctuating charge model for boron nitride networks

Angus Heafield ; Mark Wilson

J. Chem. Phys. 164, 024705 (2026)
https://doi.org/10.1063/5.0311291

The Journal of Chemical Physics ARTICLE pubs.aip.org/aip/jcp

The application of a fluctuating charge model for boron nitride networks

Cite as: J. Chem. Phys. 164, 024705 (2026); doi: 10.1063/5.0311291
Submitted: 8 November 2025 • Accepted: 22 December 2025 •
Published Online: 13 January 2026

Angus Heafield[a] and Mark Wilson

AFFILIATIONS

Physical and Theoretical Chemistry Laboratory, Department of Chemistry, University of Oxford, South Parks Road, Oxford OX1 3QZ, United Kingdom

[a]Author to whom correspondence should be addressed: angus.heafield@chem.ox.ac.uk

ABSTRACT

A fluctuating charge model (FCM) is developed to consider two-dimensional networks of boron nitride. In the FCM, the charge on each atom site is controlled by parameters linked to the atom's electronegativity and the interactions with other atoms (the coordination environment). The charge held on each atom site is a strong function of the local (first shell) coordination environment. The site charges are shown to be in excellent agreement with those extracted from independent density-functional theory-based calculations. The behavior of the site charges is investigated as a function of the network topology and site disorder. In the first case, specific defects (both site and topological) are introduced, and the spatial "decay" of the local charge to bulk values is assessed. In the second, highly disordered (amorphous) networks are generated, and the distribution of site charges is studied as a function of the degree of topological and site disorder (characterized by the fraction of six-membered rings and mean boron–nitrogen coordination numbers, respectively). Domains of high and low charges are observed to form across a wide range of topological disorder.

I. INTRODUCTION

Boron nitride (BN) is considered a promising material due to its unique thermal, electronic, and mechanical properties with a wide range of potential applications, including water purification,[1,2] UV photodetection,[3] and structural reinforcements.[4] BN has been well-studied in three main crystalline forms: hexagonal (h-BN),[5] cubic (c-BN),[6] and wurtzite (w-BN),[7] as well as a range of synthetic structures, such as thin films,[8] nanotubes,[9] fullerene-like nanoparticles,[10] and a range of amorphous states.[11] These structures are reminiscent of their carbon analogs but with the potential additional complexity of the existence of charge separation as a result of the two different atomic species with differing electronegativities. This charge separation leads to a variety of differences in structure and properties between BN and C materials, such as h-BN favoring AA′ stacking over the AB stacking favored by graphite and h-BN having a bandgap of ~6 eV (an insulator within layers[12]), while graphite has no bandgap (a conductor within layers[13]).

The existence of two elements allows different types of defects, such as boron or nitrogen vacancies, or boron/nitrogen anti-site defects, that is, boron taking the place of a nitrogen in the lattice or vice versa. In addition, the topological disorder may be introduced. The topological disorder relates to the locations of atoms in a network structure, while site-based disorder is related to how the different types of atoms occupy those sites.

We have previously found that systematically varying the charge separation, such that the *magnitude* of the charge on each site is fixed, in amorphous BN systems leads to changes in partial structure factors and radial distribution functions, while the corresponding total functions remain near-constant, indicating that there is a change in the site-based disorder, while the topological disorder remains fairly constant.[14] However, it is likely that the site charge varies according to the environment of a given atom rather than all atoms having the same charge. It is possible that this distribution of charge throughout a system could also help understand properties such as its permeability for charged species, such as, for example, ions in water desalination[15] or DNA sequencing.[16] In addition, the charge distribution may affect the movement of defects through the network.[17,18] However, establishing the precise values of the site charges remains problematic. *Ab initio* calculations suggest charges of magnitude $|q| \sim 0.25 - 0.50e$.[19] Furthermore, site charges inferred from density-functional-based calculations appear

to depend heavily on the details of the applied model, while the effect of using different charges is hard to resolve from experimental diffraction data.[14,20,21]

The fluctuating charge model, FCM, allows for the variation of charge on each site throughout a classical molecular dynamics simulation. By assigning each site an effective electronegativity, which is a function of the atom identity and its local environment, charge can move between sites depending on changes in the environment. The FCM has been used previously to model the charges on isolated molecular species, such as polyatomic anions, for example, CN^-,[22] NO_3^-,[23,24] and CO_3^{2-},[25,26] uncovering complex ordering on multiple length-scales, for example, low-dimensional chains in Na_2CO_3.[25] In this paper, we apply the FCM to much larger BN networks, allowing for the investigation into how the topological and site disorder affect the charge distributions in these systems.

The aim of this paper is to develop a model to investigate how the charge distribution in BN is affected by both topological and site disorder. We will develop and apply a fluctuating charge model to a range of two-dimensional configurations, ranging from the ideal crystalline structures to defective crystals, clusters, and disordered (amorphous) environments. The cluster calculations allow for direct comparison with the results of independent electronic structure calculations, which help validate our model parameterization. This paper is arranged as follows: The FCM is introduced, and the parameterization is established. The charges obtained are then compared to independent *ab initio* results across a range of clusters containing B, C, and N atoms. Pure BN networks are then considered, first via the introduction of specific defects leading to site and/or topological disorder, and then to highly disordered (amorphous) networks. The results are brought together in discussions, and conclusions are drawn.

II. METHODS

In this section, we will review the basis of the fluctuating charge model (FCM). We first show how the model can be modified to account for the lack of well-defined molecules, how the charge can be modified dynamically, and how the model is parameterized. We then move on to describe the methods employed to study the networks, both in terms of their generation and their dynamic evolution.

A. The fluctuating charge model (FCM) applied to continuous networks

The following derivations are based on the work of Ribeiro and Almeida,[23] Rappé and Goddard,[27] and Rick *et al.*:[28]

1. The basic model

The energy of an atom A can be expressed as a function of the atomic charge, q_A, in terms of the deviation from a neutral state, A_0,

$$E_A(q_A) = E_{A_0} + q_A\left(\frac{\partial E}{\partial q_A}\right)_{A_0} + \frac{1}{2}q_A^2\left(\frac{\partial^2 E}{\partial q_A^2}\right)_{A_0} + \cdots. \tag{1}$$

By substituting $q_A = +1, 0$, and -1 into Eq. (1) and including only terms up to the second order, the following expressions for the energy of the neutral atom and the mono-charged ions are obtained:

$$E_A(+1) = E_{A_0} + \left(\frac{\partial E}{\partial q_A}\right)_{A_0} + \frac{1}{2}\left(\frac{\partial^2 E}{\partial q_A^2}\right)_{A_0}, \tag{2}$$

$$E_A(0) = E_{A_0}, \tag{3}$$

$$E_A(-1) = E_{A_0} - \left(\frac{\partial E}{\partial q_A}\right)_{A_0} + \frac{1}{2}\left(\frac{\partial^2 E}{\partial q_A^2}\right)_{A_0}. \tag{4}$$

Equations (2)–(4) can then be used to obtain expressions for the first and second derivatives of the energy with respect to the charge,

$$\left(\frac{\partial E}{\partial q_A}\right)_{A_0} = \frac{1}{2}(IP + EA) = \chi_A^0 \tag{5}$$

and

$$\left(\frac{\partial^2 E}{\partial q_A^2}\right)_{A_0} = (IP - EA) = J_{AA}^0, \tag{6}$$

where $IP = E_A(+1) - E_A(0)$ is the ionization potential of atom A, $EA = E_A(0) - E_A(-1)$ is the electron affinity of atom A, χ_A^0 is the electronegativity of atom A in a neutral reference,[29] and J_{AA}^0 is the hardness parameter of atom A in a neutral reference.[28,30] Equations (5) and (6) can then be inserted into Eq. (1), again including only terms up to the second order, to reach an expression for the energy of atom A, using physically understandable parameters,

$$E_A(q_A) = E_{A_0} + \chi_A^0 q_A + \frac{1}{2}J_{AA}^0 q_A^2. \tag{7}$$

To calculate the optimal charge distribution in a system with more than one atom, the inclusion of the interatomic electrostatic energy, $\sum_{A<B} q_A q_B J_{AB}$, is required, where J_{AB} is the Coulombic interaction between unit charges on atoms A and B, which is dependent on r_{AB}, the distance between atoms A and B. This leads to a total electrostatic energy for a system of N atoms,

$$E(q_1 \ldots q_N, r_1 \ldots r_N) = \sum_A \left(E_{A_0} + \chi_A^0 q_A + \frac{1}{2}q_A^2 J_{AA}^0\right) + \sum_{A<B} q_A q_B J_{AB}. \tag{8}$$

Taking the derivative of Eq. (8) with respect to q_A leads to an expression for the electronegativity of atom A in the system of N atoms,

$$\chi_A(q_1 \ldots q_N, r_1 \ldots r_N) = \chi_A^0 + J_{AA}^0 q_A + \sum_{B\neq A} J_{AB} q_B. \tag{9}$$

For molecular systems, Eq. (9) can then be further divided by considering the J_{AB} term for intermolecular interactions as taking the form of the interaction between point charges, $1/r_{AB}$,[23] giving

$$\chi_{iA}(q_1 \ldots q_N, r_1 \ldots r_N) = \chi_{iA}^0 + J_{AA}^0 q_{iA} + \sum_{B\neq A} J_{AB} q_{iB} + \sum_{j\neq i}\sum_B \frac{q_{jB}}{r_{AB}}, \tag{10}$$

where $\chi_{iA}(q_1 \ldots q_N, r_1 \ldots r_N)$ is the electronegativity of atom A in molecule i.

In treating molecular systems, the breakdown in terms of intra- and inter-molecular interactions is clear. As a result, the charge may fluctuate across a given molecule with the clear constraint that the overall charge on that molecule is fixed. In a network system, the

overall system charge remains fixed; however, a length-scale needs to be identified over which the charge is allowed to effectively move. To apply the FCM to a continuous network, this length-scale is imposed by treating only atoms within a specified cutoff as allowing charge transfer, preventing charge from being transferred across longer (non-physical) distances. Equation (10) is modified as

$$\chi_A = \chi_A^0 + J_{AA}^0 q_A + \sum_{B\neq A} F_c(r_{AB}) J_{AB} q_B + \sum_{B\neq A} \left(1 - F_c(r_{AB})\right) \frac{q_B}{r_{AB}}, \quad (11)$$

where $F_c(r)$ is the cutoff complementary error function, which varies from 0 to 1,

$$F_c(r_{AB}) = \frac{1}{2}\,\mathrm{erfc}(\xi(r_{AB} - r_c)).$$

The parameter ξ is used to control how steep the cutoff is, and r_c is the cutoff radius and is the value of r for which $F_c(r)$ is equal to 0.5. A complementary error function was chosen to be modified due to its smooth and integrable nature for all values of r_{AB}, allowing for simple calculation of the forces on the charges and for the ease with which the shape of the function can be adjusted with only two parameters.

2. The movement of charge

For a system to be at equilibrium, all atomic chemical potentials must be equal. This leads to $(N-1)$ constraints on the atomic chemical potentials, or electronegativities, such that

$$\chi_1 = \chi_2 = \cdots = \chi_N. \quad (12)$$

An additional constraint arises from the requirement for charge conservation,

$$q_{tot} = \sum_{A=1}^{N} q_A, \quad (13)$$

which leads to N simultaneous equations, which can then be solved for a given structure to reach a self-consistent equilibrium set of charges. To allow for the study of dynamic systems, Rick *et al.*[28] developed a method to allow charges to evolve in time in parallel to the atom motion (a Car–Parrinello method[31]). The constraints are treated using the undetermined multipliers method, giving

$$L = \sum_{A=1}^{N_{atom}} \frac{1}{2} m_A \dot{r}_A^2 + \sum_{A=1}^{N_{atom}} \frac{1}{2} M_q \dot{q}_A^2 - E(q_1 \ldots q_N, r_1 \ldots r_N) - \lambda\left(\sum_{A=1}^{N_{atom}} q_A - q_{tot}\right), \quad (14)$$

where m_A is the mass of atom A and M_q is a fictitious charge "mass" with units of energy time^2/charge^2. Solving by the standard approach leads to the following expression:

$$M_q \ddot{q}_A = -\frac{\partial E[(q),(r)]}{\partial q_A} - \lambda = -\tilde{\chi}_A - \lambda, \quad (15)$$

showing the charges evolving in time in parallel to the atomic degrees of freedom. It is then possible to solve for λ as the total charge is fixed, such that

$$\sum_{A=1}^{N_{atom}} \ddot{q}_A = 0. \quad (16)$$

Substitution of Eq. (15) into Eq. (16) gives

$$\lambda = -\frac{1}{N_{atom}} \sum_{A=1}^{N_{atom}} \tilde{\chi}_A = -\chi_{avg}, \quad (17)$$

which can then be substituted back into Eq. (15) to give a final equation of motion,

$$\ddot{q}_A = -\frac{1}{M_q}(\tilde{\chi}_A - \chi_{avg}). \quad (18)$$

The fictitious mass, M_q, is chosen such that the charge "motion" is rapid (by comparison to the atomic motion), which allows the charges to remain at their equilibrium (adiabatic) values. In reality, although the energy transfer between the (relatively) low frequency atomic vibrational modes and the high frequency modes associated with the charges is small (reflecting the small overlap in resonant frequencies), it is not zero. As a result, if uncorrected, then energy would (slowly) transfer between the atomic modes and the (necessarily cold) charge modes, which will lead to both a decrease in the system temperature and an increase in the temperature associated with the charge motion, the latter of which corresponds to the charges becoming more detached from the required adiabatic surface. A simple way to control this (slow) energy transfer (and employed here) is to utilize Nosé–Hoover thermostats to maintain the temperature of the respective atomic and charge degrees of freedom.[32,33]

3. Parameterization

The parameters for the FCM used in this work, as shown in Table I, were adapted from those previously used to model the charges for C and O in Ref. 25. While parameters have been proposed for a range of atoms, including N,[27] these parameters were calculated for individual atoms, and so additional *ab initio* calculations are required for their application to molecules. Due to the similarity in electronegativity difference and bonding between C–O and B–N, it is believed that these parameters will also provide a good model for the charges in BN systems. The hardness parameters, J_{BB}^0

TABLE I. Parameters for the FCM for BN and C. All values are quoted in atomic units.

χ_B^0	0.200
χ_N^0	0.321
χ_C^0	0.261
J_{BB}^0	1.297
J_{NN}^0	1.474
J_{CC}^0	1.385
J_{BB}	0.226
J_{BN}	0.290
J_{NN}	0.226
J_{BC}	0.290
J_{NC}	0.290
J_{CC}	0.226

and J^0_{NN}, were adjusted to give an average absolute charge, $\overline{|q|}$, in h-BN of 0.31e, in line with previous *ab initio* calculations,[19] to allow for a meaningful comparison.

B. Methodology

Two-dimensional amorphous BN configurations were generated through the use of Monte Carlo simulations. First, topological disorder was introduced into a hexagonal network of 800 atoms through the use of a bond-switching algorithm as described in Refs. 34 and 35. The Monte Carlo move for this algorithm is the creation of a Stone–Wales defect by rotating a selected bond by 90°. This results in two rings increasing in size by one and two rings decreasing in size by one; for example, four 6-membered rings become two 5-membered rings and two 7-membered rings. To ensure a wide distribution of ring sizes, simulated annealing was utilized, wherein all Monte Carlo moves are initially accepted and then the system is "cooled down" by reducing the probability of accepting unfavorable moves. By controlling the probability of accepting moves, we are able to control the level of topological order in the system. For the configurations studied in this work, the initial thermalization was carried out over 1000 steps, followed by 10 000 steps for the "cooling" process. The networks generated are entropically driven, meaning that the resulting distributions of ring sizes follow a maximum entropy distribution. As a result, a fraction of a single ring size, usually taken as the fraction of six-membered rings, p_6, is all that is required to define the distribution since this will relate directly to the width of the distribution (Lemaître's law[36]).

The bond-switching algorithm controls the network topology and so does not take into account the identities of the atoms at each site. As a result, the bond-switching is followed by a second Monte Carlo procedure to control the site-ordering. This second algorithm involves assigning atomic identities at random to the sites and then swapping atom pairs at random. The local coordination environment is a key indicator of the level of site disorder; for example, using the mean nearest-neighbor coordination number, $\overline{n}^{\beta}_{\alpha}$, which gives the mean average number of atoms of type β in the first coordination shell of an atom of type α. Therefore, in ideal h-BN, a site-ordered three-coordinate system, $\overline{n}^{N}_{B} = \overline{n}^{B}_{N} = 3$ and $\overline{n}^{N}_{N} = \overline{n}^{B}_{B} = 0$. In the second MC procedure, the only accepted moves are those that result in an increase in the number of B–N nearest-neighbors ($\overline{n}^{N}_{B} = \overline{n}^{B}_{N}$ increases). MC moves are performed until $\overline{n}^{N}_{B}\,(= \overline{n}^{B}_{N})$ reaches a fixed value.

Finally, the systems were geometrically relaxed through the use of a steepest descent algorithm. The forces on the atoms were calculated using a Tersoff potential[37] parameterized for low-dimensional BN[38] and BN-C[39] nanostructures, augmented with the FCM for the electrostatic interaction. The molecular dynamics simulations were carried out in the N, V, T canonical ensemble at 300 K, controlled using a Nosé–Hoover thermostat. The time step was set to be 1 fs, and periodic boundary conditions were applied in the x–y plane.

III. RESULTS

A. Comparison to density-functional theory-based calculations

In order to assess the validity of our (physically motivated) parameterization, a comparison is made to the site charges obtained from recent DFT-based calculations.[40] DFT calculations were performed as described in Ref. 41 on seven two-dimensional clusters, all containing 252 atoms, of which 36 are H atoms placed on the cluster extremities to retain full (three) coordination of the B, C, and N atoms. The number of C atoms was varied from 0 (i.e., all BN) to 216 (all C) with the total number of B, N, and C atoms fixed at 216. Configurations are labeled as BN (the ideal BN lattice) or C_n, where n is the number of C atoms in the configuration, with the remaining $(216 - n)$ atoms being BN. Each configuration can be characterized in terms of both the stoichiometry (the number of B, N, and C atoms) and the local coordination environments. All sites are three-coordinate, and so the local environment can be characterized ideally by the identity of the central atom and the three nearest-neighbors. For example, the ideal BN lattice will contain B–N_3 and N–B_3 units only. Calculations were performed as described in Refs. 40 and 41, with an analysis of the site charges performed as in Ref. 41. Site charges are extracted at the MDC-q level. Analogous calculations were performed using the FCM as parameterized above, but using a periodically repeating lattice rather than the isolated cluster. Figure 1 shows an example C_{24} cluster (containing 24 C atoms) used in the DFT calculations and the periodic analog used in the FCM calculations. In both panels, the charges are highlighted via the coloring of the sites.

Figure 2 shows the distribution of site charges for the B, N, and C atoms determined for the seven cluster stoichiometries

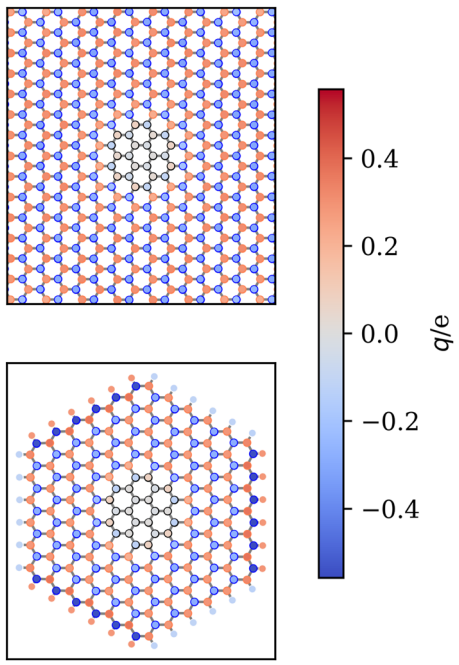

FIG. 1. Example charge "heat maps" obtained from the fluctuating charge model (top, using a periodic cell) and density-functional theory calculations (bottom, using a cluster) for systems containing 24 C atoms per cell. In both panels, the degree of red and blue corresponds to the size of the positive and negative charges, respectively. In the lower panel, the smaller circles around the edge represent the H atoms required to charge-balance the cluster. In both panels, the circle circumferences are colored red, blue, or black to indicate B, N, or C atoms, respectively.

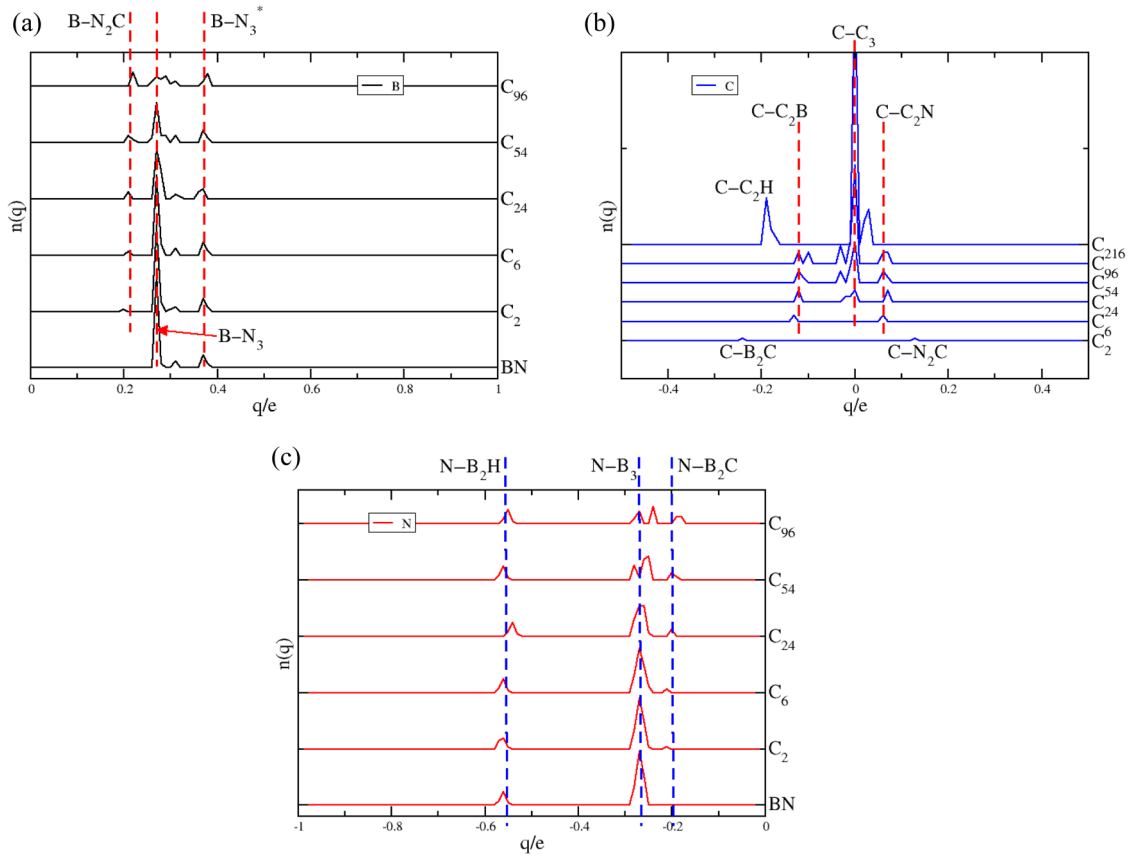

FIG. 2. Distribution of site charges obtained using density-functional theory.[41] Panels (a), (b), and (c) show the charges on the B, C, and N atoms, respectively, with the cluster composition shown on the right hand side of each panel. The vertical dashed lines are a guide to the eye and are labeled with the respective local coordination environments. The peaks labeled "B–N_3^*" in panel (a) refer to the B atoms on the edge of the cluster, which are surrounded by N atoms that are themselves nearest-neighbors to the outer H atoms.

considered, split into three panels according to atom identity. For the C atom sites, the pure BN configuration is omitted, while for the B and N sites, the pure C configuration is similarly omitted. The most significant conclusion to draw from these figures is that the charge on a given site appears to be a *strong* function of the *local* (nearest-neighbor) coordination environment. For the C atom, for example, the C_6 to C_{96} configurations show clear peaks attributable to the C–C_2B, C–C_3, and C–C_2N local coordination environments. The C_2 configuration shows peaks attributable to the C–B_2C and C–N_2C environments, while the C_{216} configuration shows peaks attributable to the C–C_3 and C–C_2H environments. Similarly, the B atom sites show peaks associated with B–N_3, B–N_2C, and B–N_2H environments, while the N atoms show the equivalent N–B_3, N–B_2C, and N–B_2H environments. In addition, a small number of B atoms show a large charge, which is the result of the next-nearest neighbors in which they are surrounded by three N atoms, but those N atoms are nearest-neighbors to the outer H atoms [labeled B-N_3^* on panel (a)]. Table II lists the mean charges and standard deviations on each site, averaged over all configurations containing those sites. In the cluster used for the DFT calculations, H atoms sit at the extremities in order to preserve charge neutrality. As a result, the DFT configurations contain both N–B_2H and B–N_2H local coordination environments.

To consider the effect of the local coordination environment on the atom charge, a careful nomenclature is required. For example, the environment about an atom of type α, surrounded by a maximum of two atom types, β and γ, may be characterized either in terms of n_α^β or n_α^γ, for which $n_\alpha^\beta + n_\alpha^\gamma = 3$. A consistent nomenclature is required to define a site α having a coordination $n_\alpha^{\beta,\gamma}$, where the numerical value is the number of atoms of type β surrounding site α (the remaining atoms being of type γ), and to order the superscripts with the most electronegative element first (i.e., $\chi_\beta > \chi_\gamma$).

Figure 3 shows the evolution of the site charge as a function of the local environment for both the DFT and FCM calculations, with the charges determined as the mean values averaged over the seven configurations studied. The error bars show the standard deviations resulting from this averaging. The figure highlights the clear dependence of, and trends in, the site charges on the local coordination environment. In addition, the relatively small standard deviations indicate that the site charges are very strongly dependent on the *local* coordination environment and not on the overall

TABLE II. Mean charges and the associated standard deviations of atom site charges obtained from density-functional theory, arranged by coordination environment as indicated in the first column. The charges are averaged across all configurations containing those local environments.

Site coordination	$\bar{q}/e$	σ_q/e
B–N_3	0.298 24	0.042 14
B–N_2C	0.217 61	0.004 90
B–N_2H	0.289 60	0.018 49
C–B_2C	−0.247 36	N/A
C–C_2B	−0.119 84	0.007 64
C–N_2C	0.137 08	N/A
C–C_2N	0.069 87	0.004 38
C–C_2H	−0.190 09	0.006 14
C–C_3	−0.000 52	0.013 62
N–B_3	−0.270 76	0.009 31
N–B_2C	−0.200 45	0.010 42
N–B_2H	−0.562 38	0.008 81
H–B	−0.105 08	0.006 57
H–C	0.162 69	0.003 66
H–N	0.292 18	0.005 18

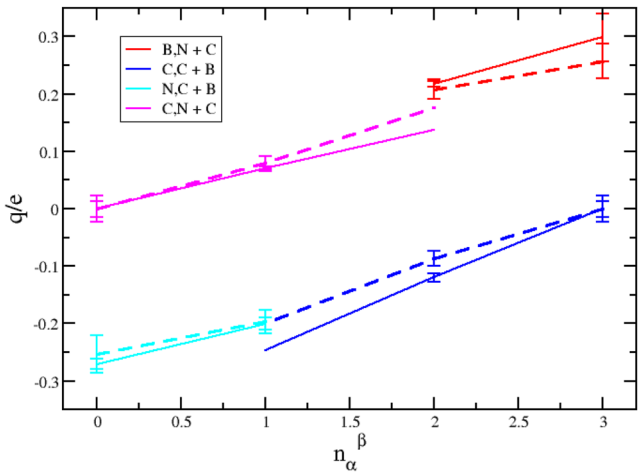

FIG. 3. Mean site charges shown as a function of the nearest-neighbor coordination environment, n_α^β. The solid and dashed lines show the results from the density-functional theory and fluctuating charge model calculations, respectively. The error bars for the DFT results reflect the differences in site charges across different stoichiometries as extracted from Fig. 2.

stoichiometry and any differences in ordering beyond the nearest-neighbor length-scale. It is clear that the FCM site charges are very close to those obtained from DFT, recalling that the FCM was *not* parameterized using the DFT values. As would be expected physically, the magnitude of the site charges becomes larger as a greater number of atoms with a larger electronegativity difference are added.

Table III shows the comparison of the nearest-neighbor atom separations for the BN, BC, NC, and CC pairs obtained from both the DFT and FCM for three example configurations: C_{24}, C_{54}, and C_{96}. The agreement in the bond lengths is close throughout, with the

TABLE III. Nearest-neighbor atom separations for the BN, BC, NC, and CC pairs obtained from both the DFT and FCM for three example configurations: C_{24}, C_{54}, and C_{96}.

	r_{BN}/Å		r_{BC}/Å		r_{NC}/Å		r_{CC}/Å	
C_n	DFT	FCM	DFT	FCM	DFT	FCM	DFT	FCM
24	1.433	1.447	1.441	1.535	1.441	1.415	1.439	1.425
54	1.432	1.446	1.435	1.538	1.436	1.412	1.441	1.424
96	1.432	1.442	1.438	1.540	1.438	1.405	1.436	1.425

only significant differences observed for the BC distances (of ~7%). For comparison, the BN, NC, and CC bond lengths show differences of ~ 1%, ~ 2%, and ~ 1%, respectively.

B. Network properties

In this section, the FCM is applied to two-dimensional networks containing different amounts of disorder. Two dimensional networks are studied as they allow for a clear separation of site and topological disorder while retaining connections with recent experimental insights.[20,21] Three "classes" of disorder are introduced and studied. In the first, site disorder is introduced by switching B and N sites, thus introducing homopolar bonds (here, N–N and B–B) while retaining the ideal total mean coordination number of three. The degree of disorder can be characterized, at the simplest level, by a mean local coordination number, such as $\bar{n}_B^N$. In the second, vacancies are created in the ideal lattice, while in the third, topological disorder is introduced via bond-switching.

1. Site disorder

Figure 4 shows the effect of varying the cutoff parameter (Sec. II A 1) for an ideal hexagonal lattice with varying degrees of site disorder, characterized by $\bar{n}_B^N$. Considering first the ideal ordering hexagonal lattice (for which $\bar{n}_B^N = 3$), the effect of the length-scale over which the charge transfers directly is clear. The curve shows characteristic "jumps" in the charge on the central atom as a result of consecutive shells of neighboring atoms coming into range. Below the nearest-neighbor length-scale (denoted $r_{\alpha\beta}^{(1)}$), the atoms adopt charges driven by their bare respective electronegativities (i.e., there are no interactions with other atoms). For $r_{\alpha\beta}^{(1)} < r < r_{\alpha\beta}^{(2)}$ (i.e., between the first and second nearest-neighbor length-scales in the ideal hexagonal lattice, with $r_{\alpha\beta}^{(2)} = \sqrt{3} r_{\alpha\beta}^{(1)} \sim 2.4$Å), the nearest-neighbor interactions lead to greater charge separation. For $r_{\alpha\beta}^{(2)} < r < r_{\alpha\beta}^{(3)}$ (i.e., $r_{\alpha\beta}^{(3)} = 2 r_{\alpha\beta}^{(1)} \sim 2.8$Å), the second nearest-neighbors (which, in the ideal lattice, are like charges) lead to a reduction in the mean site charge.

Figure 4 highlights the effect of introducing site disorder. The disorder is introduced by randomly swapping pairs of B and N atoms in a fixed lattice, and the degree of site disorder is characterized by the mean B–N coordination number, $\bar{n}_B^N$, for which $1.5 \leq \bar{n}_B^N \leq 3$, where the lower and upper limits represent the maximum disorder and ideal order, respectively. For ~ 1.4Å < r_{cut} < 2.4Å (i.e., for atoms in the nearest-neighbor coordination shell), as the degree of disorder increases, the effect of the nearest-neighbor and

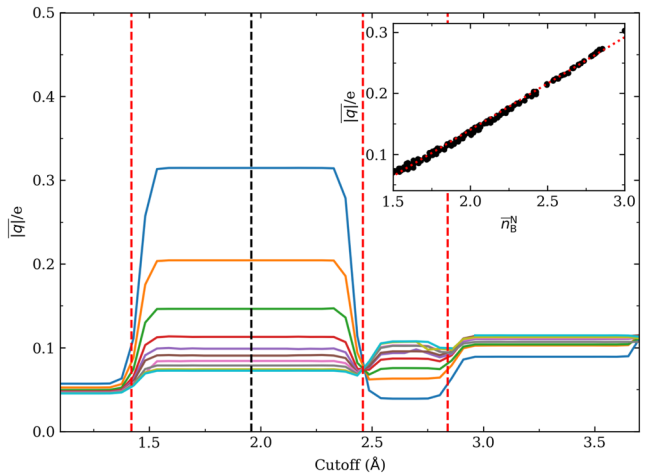

FIG. 4. (Main panel) Mean average site charge, $|\bar{q}|$, shown against the cutoff radius employed for the fluctuating charge model as described in the text. The site charges are shown for a range of site disorders on an ideal hexagonal lattice. Looking along the black vertical dashed line, corresponding to $r_{cut} = 1.96$Å, from bottom to top, $\overline{n}_B^N = 1.505, 1.507, 1.550, 1.598, 1.623, 1.707, 1.815, 2.060, 2.406, 3.000$. The inset shows the mean average site charge, $|\bar{q}|$, as a function of $\overline{n}_B^N$ for a fluctuating charge model cutoff of $r_{cut} = 1.96$Å (corresponding to the vertical black dashed line in the main panel). The red vertical dashed lines show the length-scales associated with successive coordination shells ($r_{\alpha\beta}^{(1)} = 1.4$Å, $r_{\alpha\beta}^{(2)} = \sqrt{3}r_{\alpha\beta}^{(1)} \sim 2.4$Å, $r_{\alpha\beta}^{(3)} = 2r_{\alpha\beta}^{(1)} \sim 2.8$Å).

next-nearest-neighbor interactions diminishes. The inset to the figure shows the mean site charge as a function of the mean coordination number with a cutoff intermediate between the first and second shells (i.e., including the interactions with the neighboring atoms only). The mean site charge shows a near-linear dependence on the local coordination number.

2. Defects

The analysis in Secs. III B 1 and III B 2 indicates how the site charge appears to be a strong function of the nearest-neighbor coordination environment. In this section, we consider the effect on the site charges of the introduction of specific defects. Three types of defects are considered: anti-site, vacancy, and Stone–Wales rotation. Figures 5(a)–5(c) show the examples of ideal hexagonal nets with a single defect. In panel (a), the B atom replaces an N (an anti-site defect); in panel (b), a single N atom is removed; and panel (c) shows a single Stone–Wales rotation. In all cases, the area of the hexagonal net is fixed at that for the energy minimum of the ideal net. The ideal defect is generated, and the atom positions are relaxed using a steepest descent algorithm. To highlight the effect of the site charges on the presence of the defects, Fig. 6 shows the evolution of the site charges as a function of distance away from the central defect site. Figure 6 shows the difference in charge on the site α, $|\Delta q_1| = |q - \bar{q}_{bulk}|$, with respect to the site charge at large distances from the defect (i.e., the bulk values in the ideal hexagonal lattice).

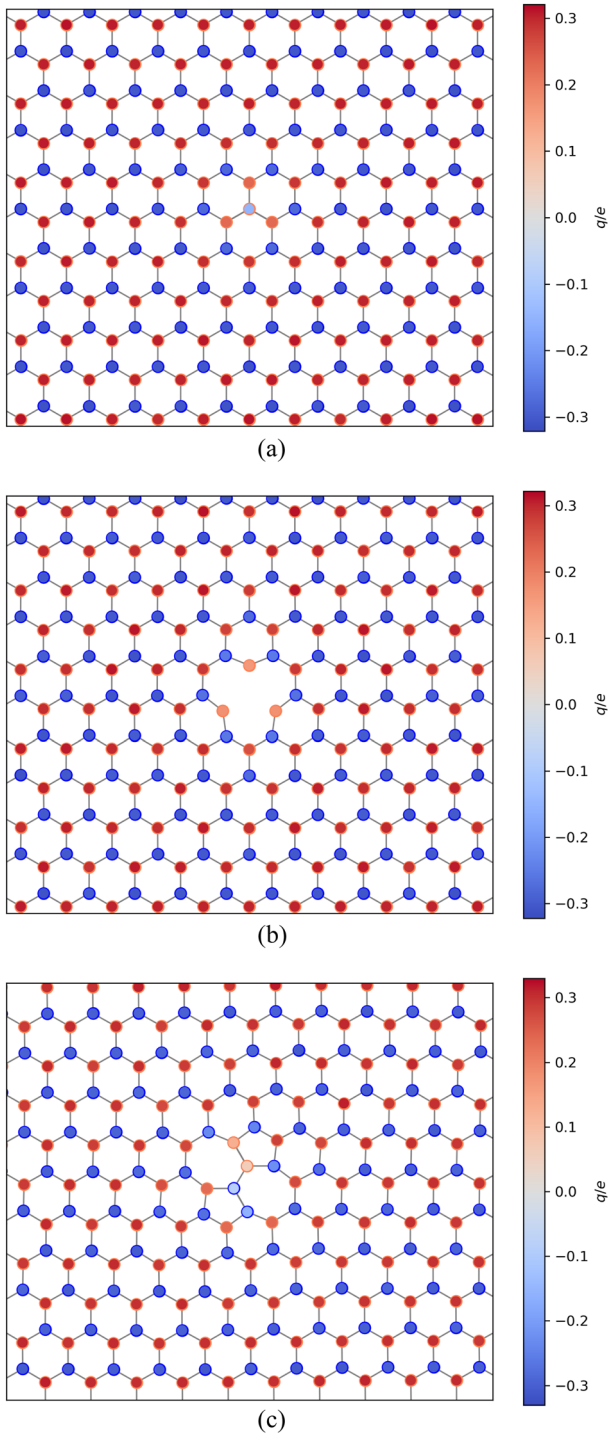

FIG. 5. Charge "heat maps" for three types of defects in an ideal hexagonal lattice. (a) A boron anti-site defect, (b) a nitrogen vacancy, and (c) a Stone–Wales defect. In all panels, the degree of red and blue corresponds to the size of the positive and negative charges, respectively. The circle circumferences are colored red or blue, which indicate B or N atoms, respectively.

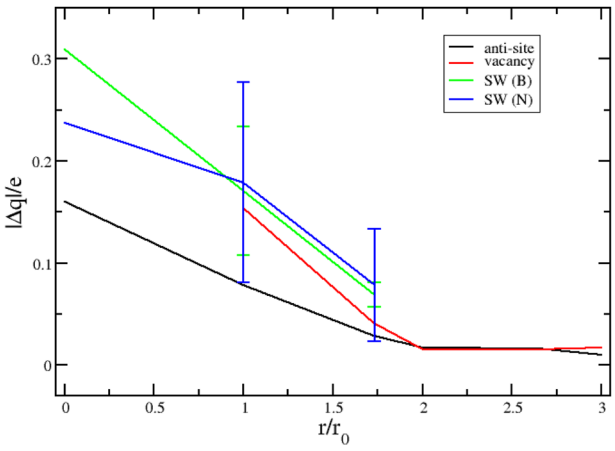

FIG. 6. Magnitudes of the mean site charge differences as a function of distance away from the defect for the B anti-site (black line), N vacancy (red line), and Stone–Wales defect with respect to the B and N atoms (green and blue lines, respectively). The distance is shown relative to the ideal B–N nearest-neighbor separation, r_0.

For the anti-site defect, the central B atom (which has replaced an N atom) adopts a small *negative* charge, reflecting the nearest-neighbor coordination environment of three B atoms (which adopt positive charges, but smaller than those observed in the bulk environments). The site charge "relaxes" to the bulk values by around $r/r_0 \sim 2$ (i.e., by the third coordination shell). For the N vacancy, the nearest-neighbor B atoms again adopt a smaller positive charge than for the bulk equivalents, with the charges again effectively reaching their bulk values by the third coordination shell with $r/r_0 \sim 2.6$. For the SW defect, we can consider the charges at a distance with respect to either the B or N atoms in the bond, which has been switched. Note that the presence of topological disorder almost certainly links to site disorder (unless the network retains only even-membered rings). In both cases, the charge decays to the bulk value by $r/r_0 \sim 3$.

3. Topological disorder

Figure 7(a) shows the examples of the distribution of site charges on the B and N atoms "colored" by the fraction of six-membered rings, p_6, with $p_6 = 0.35, 0.50, 0.65$, and 0.80. The distribution of charges appears near-independent of the degree of topological disorder. Note that a small fraction of atoms (of the order of 2%–4%) adopt the opposite charge to that suggested by their formal valence. The charge distributions highlighted in Fig. 7(a) can be further colored in terms of the local coordination environment. Figure 7(b) shows an example breakdown of the charges on the B and N atoms for a configuration with $p_6 = 0.5625$ and $\overline{n}_{\mathrm{B}}^{\mathrm{N}} = 2.19$ and highlights the clear separation of charge based on local environment as displayed in Fig. 3. It is clear that the strong dependence of the site charge on the *local* coordination environment identified in Secs. III B 1 and III B 2 in more idealized structures persists into more disordered states.

Figure 8 shows the three example amorphous configurations, which display different levels of disorder as quantified by the fraction of six-membered rings, $p_6 = 0.37$, 0.56, and 0.82, respectively.

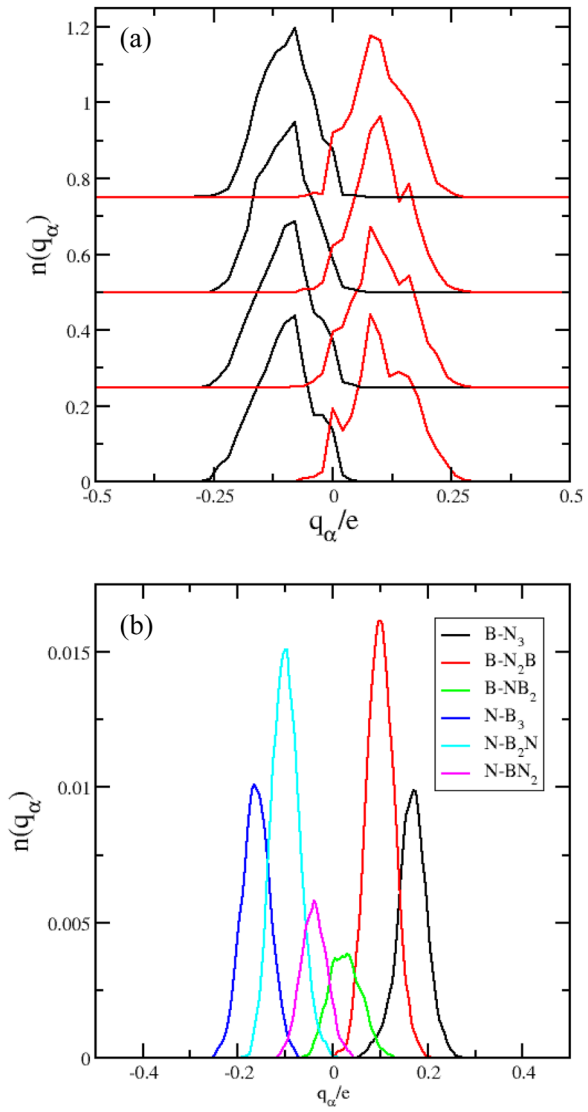

FIG. 7. (a) Distribution of site charges on the B (red lines) and N (black lines) atoms for disordered networks at four different levels of disorder as characterized by the fraction of six-membered rings, p_6, from bottom to top, $p_6 = 0.35, 0.50, 0.65, 0.80$. Successive distributions are offset along the abscissa for clarity. (b) An example charge distribution for the amorphous network with $p_6 = 0.5625$ broken down in terms of the local coordination environment as indicated in the legend.

Panel (a) shows the charge map for $p_6 = 0.56$, with the atom colors indicating the degree of positive or negative charge on those sites (i.e., highly positively charged B atoms appear more red, and highly negatively charged N atoms appear more blue). Panels (b), (c), and (d) show an alternative representation for $p_6 = 0.37$, 0.56, and 0.82, respectively, with the intensity of the color indicating a deviation of the absolute charge from the mean value, $\Delta q_2 = |q| - \overline{|q|}$. It appears visually that there are regions of relatively high and low charges, spread over groups of atoms, across all levels of topological disorder. To attempt to characterize these regions, partial structure factors

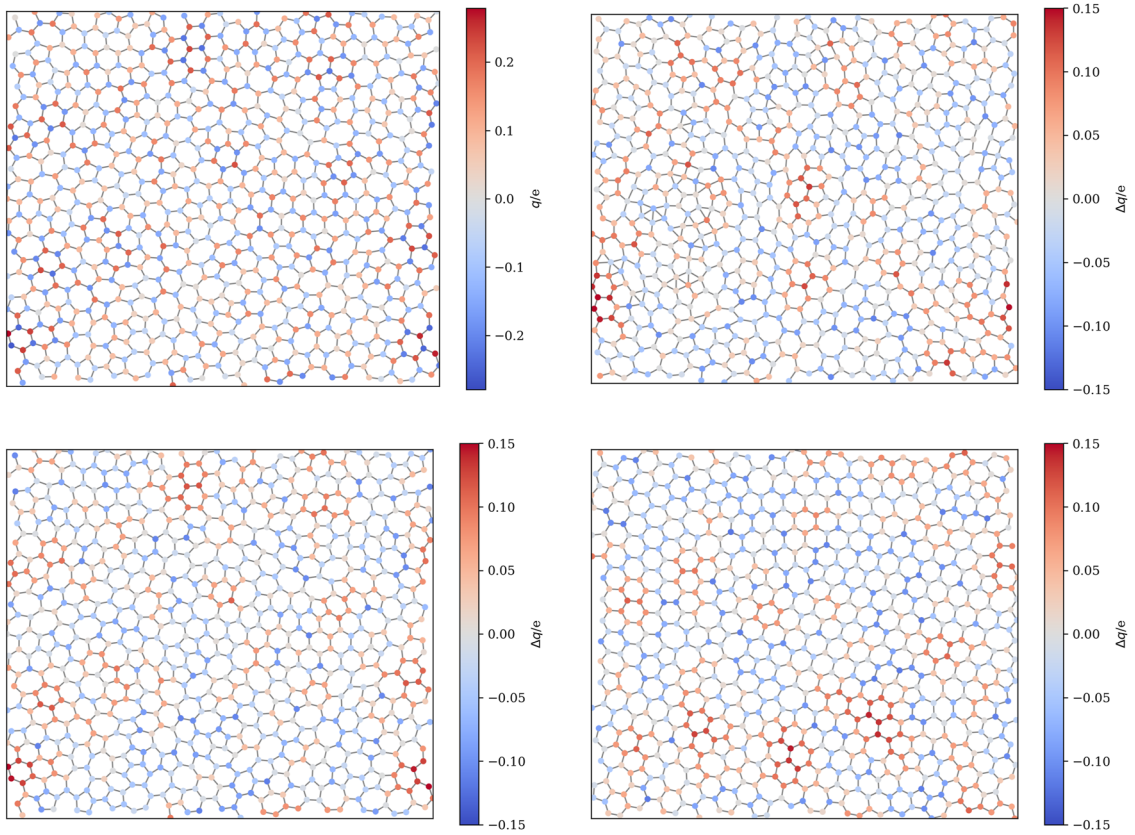

FIG. 8. Charge "heat maps" for three example configurations with a range of p_6 values. The top-left panel shows a configuration with $p_6 = 0.5628$, and the atoms are colored based on their partial charges, q, with the degree of red and blue indicating more positive and negative charges, respectively. The top-right, bottom-left, and bottom-right panels show the configurations with $p_6 = 0.3659$, 0.5628, and 0.8241. The atoms in these panels are colored based on their Δq values, $\Delta q = |q| - \overline{|q|}$, with the degree of red and blue indicating more positive and negative values, respectively.

are constructed, which are colored by the magnitude of the charges on each site. The distribution of charge magnitudes is divided into high and low charges using the distributions of the type shown in Fig. 7. The 20% of the atoms with the highest charge magnitudes are labeled "high" (h), and the remaining 80% are labeled "low" (l). Partial structure factors and radial distribution functions are extracted from these two groups of configurations, for example,

$$S^{Q}_{\alpha\beta}(k) = \langle A^{*}_{\alpha}(k).A_{\beta}(k)\rangle, \tag{19}$$

where $A_\alpha(k) = \frac{1}{\sqrt{N_\alpha}}\sum_i e^{i\mathbf{k}\mathbf{r}_i}$ is the Fourier component, and α and β refer to the high and low charge atoms, respectively. Figures 9(a) and 9(b) show $S^{Q}_{\alpha\beta}(k)$ for $\alpha\beta = hh, hl, ll$ calculated over two p_6 domains, $0.3 < p_6 < 0.4$ and $0.7 < p_6 < 0.8$. The effect of increasing the level of disorder (reducing p_6) is clear in all three partial structure factors. The functions at high p_6 show significantly sharper peaks, and some clearly coalesce to form single peaks at low p_6. Similar changes have been observed in two dimensional networks of amorphous carbon.[42] To help understand the distribution of charge in the networks, Figs. 9(a) and 9(b) show the analogous partial structure factors obtained by assigning the "h" and "l" labels at random (rather than by charge magnitude). As a result, the three partial structure factors become equivalent and differ only in the fluctuations due to the small number of sites labeled "h." The most striking difference between the different functions is in $S^{Q}_{hh}(k)$, which shows significant intensity at low k, indicative of the formation of nanodomains of the sort shown in Fig. 8. Analogous partial radial distribution functions can also be defined. Figures 9(c) and 9(d) show $g^{Q}_{\alpha\beta}(r)$ for $\alpha\beta = hh, hl, ll$ [the analogs of the structure factors shown in panels (a) and (b)] again colored in terms of site charge and at random. The greater ordering at high p_6 is again clear in terms of sharper peaks and oscillations persisting to significantly higher r. More significantly, here the formation of the charge domains is evident, most clearly in $g^{Q}_{hh}(r)$, which shows significantly greater intensity in both the first and second peaks.

To focus a little more on these domains, Fig. 10 shows $S^{Q}_{hh}(k)$ calculated over six different ranges of p_6 using the labeling by charge [panel (a)] and at random [panel (b)]. The greater ordering as p_6 increases is again clear across both sets of functions. For the charge-labeled functions [panel (a)], the low k intensity shows a small increase as p_6 increases. An approximate measure of the spatial extent of the charge domains can be extracted by relating the low

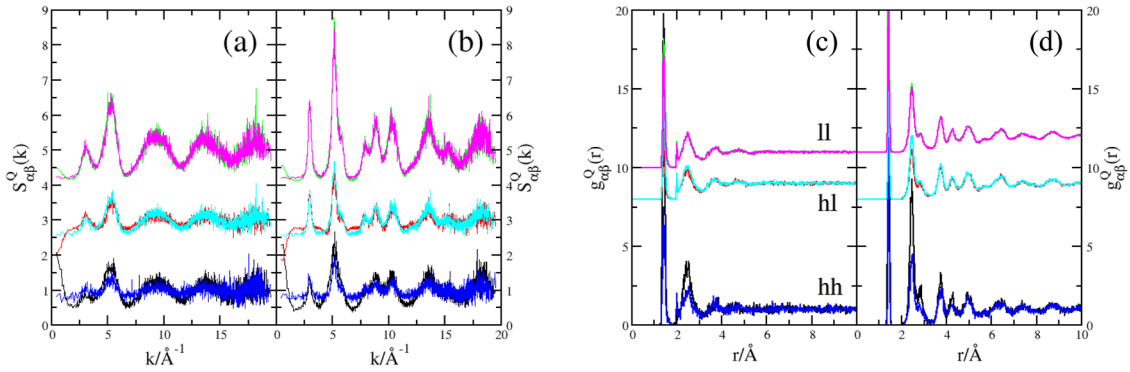

FIG. 9. Panels (a) and (b) show the structure factors, $S^{Q}_{\alpha\beta}(k)$, colored in terms of high and low charges (labeled "h" and "l," respectively, as discussed in the main text). The black, red, and green lines show $S^{Q}_{hh}(k)$, $S^{Q}_{hl}(k)$, and $S^{Q}_{ll}(k)$, respectively. The blue, cyan, and magenta lines show the equivalent functions but with the atoms labeled at random as described in the text. Successive functions are offset along the abscissa axis for clarity. Panels (c) and (d) show the corresponding partial radial distribution functions, which employ the same color scheme as panels (a) and (b).

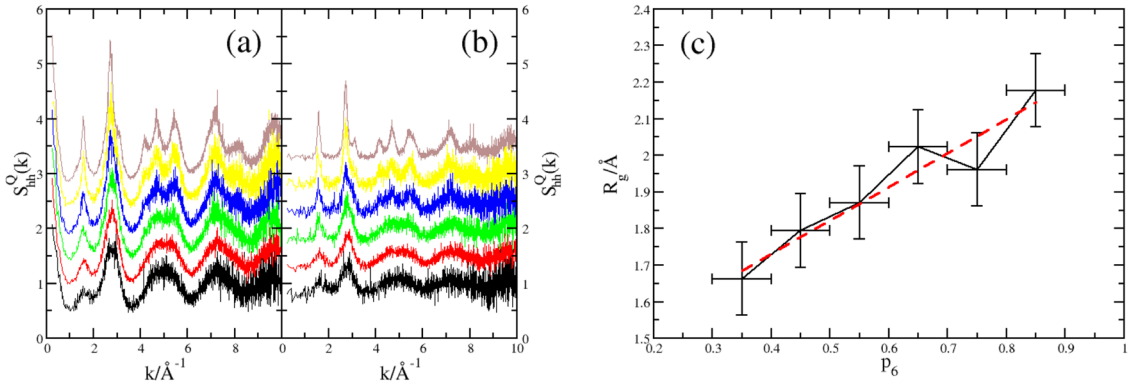

FIG. 10. Panels (a) and (b) show the structure factor, $S^{Q}_{hh}(k)$, colored in terms of high charge as described in the main text. In both panels, successive functions are determined at different levels of disorder as characterized by the fraction of six-membered rings, p_6. Successive functions are offset along the abscissa axis for clarity. From bottom to top, $0.3 < p_6 < 0.4$, $0.4 < p_6 < 0.5$, $0.5 < p_6 < 0.6$, $0.6 < p_6 < 0.7$, $0.7 < p_6 < 0.8$, and $0.8 < p_6 < 0.9$. Panel (a) shows the effect of coloring the sites by high charge, while panel (b) shows the analogous functions generated by selecting the same fraction of sites at random. Panel (c) shows the effective radius of the domain size as a function of the fraction of six-membered rings determined from the low $-k$ gradient as described in the text.

k gradient to an effective radius of gyration (i.e., by plotting the low k regime against k^2 and extracting the gradient). Figure 10(c) shows the change in domain radius as a function of p_6, highlighting the weak increase in domain size as the level of disorder is reduced.

IV. DISCUSSION

The results presented here show how the charge held by each atom can fluctuate as a function of the atom's environment. In the present work, a relatively simple network system (BN) has been chosen. The environment here is effectively synonymous with network disorder, which is present here in the form of both site and topological disorder. It is clear that the charge separation, resulting from the difference in electronegativities of the two atomic species, is both significant and highly dependent on the local coordination environment. While using fixed (mean field) values for the charges is possible, it is likely to lead to significant errors, in particular where there are high levels of disorder (either pure site or topological/site disorder). These errors are likely more significant in systems such as BN, in which the charge *magnitudes* are relatively small and, hence, the effect of the (local) environment is potentially more important.

Future work will focus on a number of key extensions. The formation of large pores in these systems is of general interest, as these thin films can act as filters (for example, in desalination). The implication of the present work is that the charge present on atoms sitting on the pores may be significantly different from those in the bulk, with clear implications for properties such as ion transport. Adding a third atom type (for example, carbon to form BCN composites) introduces additional significant complexity with the potential formation of superlattices in which the carbon atoms effectively remain demixed, forming domains. The potential changes in charge indicate that the addition of intercalated atoms or molecules may alter the charge distribution in a significant manner. In

addition, it is likely that similar charge separation effects will be observed in three-dimensional networks and in BN nanotubes and fullerenes.

V. CONCLUSIONS

In this paper, a fluctuating charge model (FCM) has been developed to study a key network material, BN. In the FCM, the charge on each atomic site is controlled by the atom's electronegativity plus terms that are linked to the interactions with the surrounding environment. As a result, charges can deviate from their typical (mean field) values. The results presented here show how the introduction of simple defects, both in terms of site and topological disorder, leads to significant changes in site charge. In addition, in highly disordered (amorphous) systems, the network is arranged into regions of relatively high and low charges, with the size of the charge domains a weak function of the degree of topological disorder. The distribution in charge is likely most significant in systems such as BN in which the typical mean charge magnitudes are relatively small.

ACKNOWLEDGMENTS

This paper conforms to the RCUK data management requirements.

AUTHOR DECLARATIONS

Conflict of Interest

The authors have no conflicts to disclose.

Author Contributions

Angus Heafield: Conceptualization (equal); Data curation (equal); Formal analysis (equal); Investigation (equal); Methodology (equal); Project administration (equal); Software (equal); Supervision (equal); Validation (equal); Visualization (equal); Writing – original draft (equal); Writing – review & editing (equal). **Mark Wilson**: Conceptualization (equal); Data curation (equal); Formal analysis (equal); Investigation (equal); Methodology (equal); Project administration (equal); Supervision (equal); Validation (equal); Visualization (equal); Writing – original draft (equal); Writing – review & editing (equal).

DATA AVAILABILITY

The data that support the findings of this study are available from the corresponding author upon reasonable request.

REFERENCES

[1] L. Liu, Y. Liu, Y. Qi, M. Song, L. Jiang, G. Fu, and J. Li, Sep. Purif. Technol. **251**, 117409 (2020).
[2] X. Davoy, A. Gellé, J. C. Lebreton, H. Tabuteau, A. Soldera, A. Szymczyk, and A. Ghoufi, ACS Omega **3**, 6305 (2018).
[3] Y. Li, J. Guo, W. Zheng, and F. Huang, Appl. Phys. Lett. **117**, 023504 (2020).
[4] J. Reif, T. N. Narayanan, D. P. Hashim, N. Sakhavand, R. Shahsavari, R. Vajtai, and P. M. Ajayan, Adv. Funct. Mater. **23**, 5624 (2013).
[5] A. E. Naclerio, P. R. Kidambi, A. E. Naclerio, and P. R. Kidambi, Adv. Mater. **35**, 2207374 (2023).
[6] C. B. Samantaray and R. N. Singh, Int. Mater. Rev. **50**, 313 (2005).
[7] T. Liu, Y. Li, J. He, K. Zhang, Y. Hu, X. Chen, C. Wang, X. Huang, L. Kong, and J. Liu, J. Mater. Sci. **54**, 5366 (2019).
[8] M. J. Molaei, M. Younas, and M. Rezakazemi, ACS Appl. Electron. Mater. **3**, 5165 (2021).
[9] T. Xu, K. Zhang, Q. Cai, N. Wang, L. Wu, Q. He, H. Wang, Y. Zhang, Y. Xie, Y. Yao, and Y. Chen, Chem. Eng. J. **431**, 134118 (2022).
[10] D. V. Shtansky, K. L. Firestein, and D. V. Golberg, Nanoscale **10**, 17477 (2018).
[11] S. M. Sattari-Esfahlan, S. Mirzaei, M. J. Josline, J. Y. Moon, S. H. Hyun, H. Jang, and J. H. Lee, Nano Convergence **12**, 22 (2025).
[12] C. Elias, P. Valvin, T. Pelini, A. Summerfield, C. J. Mellor, T. S. Cheng, L. Eaves, C. T. Foxon, P. H. Beton, S. V. Novikov, B. Gil, and G. Cassabois, Nat. Commun. **10**, 2639 (2019).
[13] K. S. Novoselov, A. K. Geim, S. V. Morozov, D. Jiang, Y. Zhang, S. V. Dubonos, I. V. Grigorieva, and A. A. Firsov, Science **306**, 666 (2004).
[14] A. Heafield and M. Wilson, J. Phys.: Condens. Matter **37**, 045101 (2024).
[15] M. Zahoor, P. M. Ismail, S. Khan, M. Bououdina, M. Haneef, J. Akbar, E. Ahmed, C. Zeng, and S. Ali, "Hexagonal boron nitride for water desalination and wastewater treatment," in *Hexagonal Boron Nitride: Synthesis, Properties, and Applications* (Elsevier, 2024), pp. 457–482, ISBN: 9780443188435.
[16] L. Zhang and X. Wang, Nanomaterials **6**, 111 (2016).
[17] A. Zobelli, C. P. Ewels, A. Gloter, and G. Seifert, Phys. Rev. B **75**, 094104 (2007).
[18] N. Alem, R. Erni, C. Kisielowski, M. D. Rossell, P. Hartel, B. Jiang, W. Gannett, and A. Zettl, Phys. Status Solidi RRL **5**, 295 (2011).
[19] L. Chkhartishvili, S. Dekanosidze, N. Maisuradze, M. Beridze, and R. Esiava, East.-Eur. J. Enterp. Technol. **3**, 50 (2015).
[20] A. Govind Rajan, M. S. Strano, and D. Blankschtein, J. Phys. Chem. Lett. **9**, 1584 (2018).
[21] L. Susana, A. Gloter, M. Tencé, and A. Zobelli, ACS Nano **18**, 7424 (2024).
[22] M. C. C. Ribeiro and L. C. J. Almeida, J. Chem. Phys. **110**, 11445 (1999).
[23] M. C. C. Ribeiro and L. C. J. Almeida, J. Chem. Phys. **113**, 4722 (2000).
[24] M. C. Wilding, M. Wilson, M. C. C. Ribeiro, C. J. Benmore, J. K. R. Weber, O. L. G. Alderman, A. Tamalonis, and J. B. Parise, Phys. Chem. Chem. Phys. **19**, 21625 (2017).
[25] M. Wilson, M. C. C. Ribeiro, M. C. Wilding, C. Benmore, J. K. R. Weber, O. Alderman, A. Tamalonis, and J. B. Parise, J. Phys. Chem. A **122**, 1071 (2018).
[26] M. C. Wilding, F. Demmel, and M. Wilson, J. Phys. Chem. A **129**, 1890 (2025).
[27] A. K. Rappe and W. A. Goddard III, J. Phys. Chem. **95**, 3358 (1991).
[28] S. W. Rick, S. J. Stuart, and B. J. Berne, J. Chem. Phys. **101**, 6141 (1994).
[29] R. S. Mulliken, J. Chem. Phys. **2**, 782 (1934).
[30] R. G. Parr and R. G. Pearson, J. Am. Chem. Soc. **105**, 7512 (1983).
[31] R. Car and M. Parrinello, Phys. Rev. Lett. **55**, 2471 (1985).
[32] S. Nosé, J. Chem. Phys. **81**, 511 (1984).
[33] W. G. Hoover, Phys. Rev. A **31**, 1695 (1985).
[34] D. Ormrod Morley and M. Wilson, J. Phys.: Condens. Matter **30**, 50LT02 (2018).
[35] D. Ormrod Morley, A. Thorneywork, R. Dullens, and M. Wilson, Phys. Rev. E **101**, 042309 (2020).
[36] A. Gervois, J. P. Troadec, and J. Lemaitre, J. Phys. A: Math. Gen. **25**, 6169 (1992).
[37] J. Tersoff, Phys. Rev. Lett. **61**, 2879 (1988).
[38] C. Sevik, A. Kınacı, J. B. Haskins, and T. Çağın, Phys. Rev. B **84**, 085409 (2011).
[39] A. Kınacı, J. B. Haskins, C. Sevik, and T. Çağın, Phys. Rev. B **86**, 115410 (2012).
[40] E. M. O'Sullivan, N. Grobert, and M. Swart, J. Phys. Chem. C **129**, 638 (2024).
[41] M. Swart, P. T. V. Duijnen, and J. G. Snijders, J. Comput. Chem. **22**, 79 (2001).
[42] A. Kumar, M. Wilson, and M. F. Thorpe, J. Phys.: Condens. Matter **24**, 485003 (2012).